PCCP

ROYAL SOCIETY OF CHEMISTRY

PAPER

View Article Online
View Journal | View Issue

Cite this: *Phys. Chem. Chem. Phys.*, 2026, **28**, 7963

Thermodynamics of the glycerol oxidation reaction: effect of temperature, pH, applied potential, and concentration

Andrés F. Pérez-Torres,*[ab] Roel van de Krol [ab] and Marco Favaro *[a]

Received 23rd December 2025,
Accepted 2nd March 2026

DOI: 10.1039/d5cp05002b

rsc.li/pccp

(Photo)electrochemical glycerol oxidation (GOR) offers a promising route to pair H_2 production with the upgrading of low-value organics into valuable chemicals, yet its implementation is hindered by persistent selectivity challenges. In this work, we present a comprehensive thermodynamic analysis of the full GOR reaction network to clarify how temperature, pH, applied potential, and concentration govern product distribution. We find that temperature and concentration exert only minor influence on selectivity, while pH and applied potential play decisive roles. Elevated pH and high anodic bias substantially increase the thermodynamic accessibility of side reactions, limiting the selective formation of desired products. These results indicate that operating under acidic conditions and avoiding excessive potentials is essential for suppressing competing pathways. Overall, this thermodynamic framework provides clear, actionable guidelines for improving the selectivity and efficiency of GOR systems.

Introduction

The growing urgency to defossilize the chemical and energy sectors has prompted a global shift toward renewable and sustainable alternatives. While clean energy technologies such as solar, wind, and geothermal power have advanced significantly, they fall short in one critical aspect: providing renewable sources of organic carbon.[1] This is particularly problematic for the chemical industry, which remains heavily dependent on fossil fuel–derived hydrocarbons not only for energy but also for the foundational building blocks of commodity chemicals.[2,3] This reliance contributes substantially to CO_2 emissions and environmental degradation. Therefore, achieving a truly sustainable future requires technologies capable of delivering both clean energy and renewable carbon feedstocks. One promising strategy to address this dual challenge is hybrid (photo)-electrolysis, a process in which the oxidation of biomass-derived molecules at the anode is coupled with the hydrogen evolution reaction (HER) at the cathode.[2,4] This integrated approach enables the simultaneous production of value-added chemicals and green hydrogen, offering a synergistic route to defossilize both the chemical and energy sectors. Among biomass-derived feedstocks, glycerol (GLY) has emerged as a particularly attractive candidate. As a major byproduct of biodiesel production, glycerol is abundant, low-cost, and chemically versatile due to its rich functional group structure.[5] These properties make it well-suited for electrochemical conversion into a wide variety of value-added C_3 and C_2 products.[6] When employed in hybrid electrolysis, glycerol oxidation not only reduces the anodic overpotential compared to the oxygen evolution reaction (OER) but also facilitates the generation of high-value compounds alongside hydrogen gas.[7] Several of these oxidation products, such as glyceric acid (GLAC) and dihydroxyacetone (DHA), are widely used in the pharmaceutical, cosmetic, and food industries, having market prices far above that of crude glycerol. While these market prices exhibit a wide spread of values depending on the source used for their calculations and the accounted purity of the chemicals, the added value of the reaction still holds economic feasibility. For example, while glycerol is priced between 0.3 USD per kg (ref. 8) and 1 USD per kg,[9] GLAC and DHA can reach, at the current market demand, 800 USD per kg and between 5[10] and 150 USD per kg,[8] respectively. This substantial value difference highlights the economic potential of glycerol valorisation.

However, realizing this potential remains a major challenge. The (photo)electrochemical glycerol oxidation reaction (GOR) involves a highly complex network of competing reaction pathways that can yield a broad range of partially or fully oxidised products, often simultaneously. Achieving high selectivity toward specific high-value products, such as DHA or GLAD, requires fine control over several parameters, including electrode material,

[a] *Institute for Solar Fuels, Helmholtz-Zentrum Berlin für Materialien und Energie GmbH, Hahn-Meitner-Platz 1, 14109 Berlin, Germany. E-mail: andres.perez_torres@helmholtz-berlin.de, marco.favaro@helmholtz-berlin.de*

[b] *Institut für Chemie, Technische Universität Berlin, Straße des 17. Juni 124, 10623 Berlin, Germany*

electrolyte composition, pH, and applied potential (or photovoltage in a photoelectrochemical single/double junction device).[11] Despite recent and meaningful advances, the challenge of steering the selectivity toward a specific product in GOR continues to be a key barrier to its widespread implementation.[12] Addressing this challenge, namely understanding the factors that drive selectivity, is crucial for unlocking glycerol's role as a sustainable carbon feedstock in a defossilized and environment conscious chemical industry. In our previous work, using a simplified reaction network, we demonstrated that temperature has little influence on product selectivity, while higher applied potentials tend to favour the formation of more oxidised species.[7] In the present study, we take a step forward to understand the factors affecting selectivity. By expanding our analysis to a more comprehensive reaction network, we consider not only the primary oxidation of glycerol but also the successive re-oxidation of its intermediate products, a crucial aspect when the process is carried out in batch reactors or devices. This expanded framework enables a more realistic and mechanistic understanding of the reaction landscape. Within this scope, we examine how key process parameters such as temperature, applied potential, pH, and species concentrations, affect the oxidation potentials of the different reactions in the GOR network. Such understanding provides insight into the conditions that favour higher selectivity while minimizing the influence of side reactions.

Methods

Thermochemical properties of glycerol and its oxidation products were calculated using Aspen Plus. Because the GOR occurs in water, model selection was guided by the need to accurately describe intermolecular interactions in aqueous solutions. All calculations were conducted under the assumption of infinite dilution, such that only water–solute interactions were considered and solute–solute interactions were neglected.

Model selection followed the heuristic "don't gamble with thermochemical properties for chemical simulations", developed at the University of Texas and implemented in Aspen Plus.[13] For alcohols and small organic acids in water, the recommended methods include NRTL-NTH, NRTL-HOC, NRTL-RK, UNIFAC-DMD, and WILS-NTH. In this notation, the first term refers to the activity coefficient model used to describe liquid-phase non-ideality, while the second corresponds to the equation of state used for vapor-phase properties. NRTL denotes the non-random two-liquid model, UNIFAC the UNIversal Functional Activity Coefficients method, and WILS the Wilson equation. All candidate models were evaluated against available experimental data for glycerol oxidation products in our previous work.[7] The NRTL-NTH model provided the best agreement and was therefore selected for the final simulations.

The Gibbs free energy of formation ($\Delta_f G$) and enthalpy of formation ($\Delta_f H$) at infinite dilution in water were calculated at 1 bar over a temperature range of 25–80 °C. The required thermochemical data were obtained from the Aspen Plus databases when available. For species not included in the database, properties were estimated using the GANI group contribution method due to its demonstrated predictive accuracy.[14] This approach was applied to glyceraldehyde, glyceric acid, tartronic acid, hydroxypyruvic acid, mesoxalic acid, and glyoxylic acid.

The resulting temperature-dependent formation properties include solvation effects and were used to determine the Gibbs free energy of reaction ($\Delta_{rxn}G$) and enthalpy of reaction ($\Delta_{rxn}G$) according to eqn (2) and (3). These quantities were subsequently converted into the reversible potential (eqn (4)) and thermoneutral voltage (eqn (5)). Standard reaction values ($\Delta_{rxn}G^\circ$ and $\Delta_{rxn}H^\circ$) correspond to calculations performed at 298.15 K and 1 bar. All standard-state calculations assumed pH = 0, corresponding to fully protonated species. Potentials are reported relative to the standard hydrogen electrode (SHE), for which the standard Gibbs free energy and enthalpy of formation of H^+ are defined as zero.

$$r\mathrm{R} + m\mathrm{H_2O} \rightleftharpoons o\mathrm{O} + h\mathrm{H^+} + n\mathrm{e^-} \quad (1)$$

$$\Delta_{rxn}G = \sum o \cdot \Delta_f G_O - \sum r \cdot \Delta_f G_R + m \cdot \Delta_f G_{H_2O} \quad (2)$$

$$\Delta_{rxn}H = \sum o \cdot \Delta_f H_O - \sum r \cdot \Delta_f H_R + m \cdot \Delta_f H_{H_2O} \quad (3)$$

$$E_{rev} = \frac{\Delta_{rxn}G}{nF} \quad (4)$$

$$E_{th} = \frac{\Delta_{rxn}H}{nF} \quad (5)$$

To account for pH effects on GOR thermodynamics, a modified formulation of Nernst equation (eqn (6)) was employed. To see the derivation of the thermodynamic model please refer to Notes S1 and S2. In this framework, pH dependence arises from two contributions: (i) the pH-dependent speciation of reactants and products, given by E°(pH), and (ii) the net proton release coefficient, h. This coefficient accounts for protons generated both directly by the oxidation reaction and through the acid–base behaviour of the participating species.

$$E(\mathrm{pH}) = E^\circ(\mathrm{pH}) + \frac{RT}{nF}\left(\ln\frac{P^p}{R^r} - h \cdot \ln 10 \cdot \mathrm{pH}\right) \quad (6)$$

Results and discussion

Before focusing on the thermodynamics of GOR and its analysis, it is important to delineate the general features of the reaction network. The (photo)electrochemical glycerol oxidation can be described as an inner-sphere reaction that proceeds through a network of parallel and consecutive reaction pathways. Within this network, two principal reaction classes can be identified: heterogeneous (photo)electrochemical oxidation reactions and homogeneous reactions. The first type, which constitutes the main focus of this work and the desired pathway, occurs at the interface between the (photo)electrocatalyst

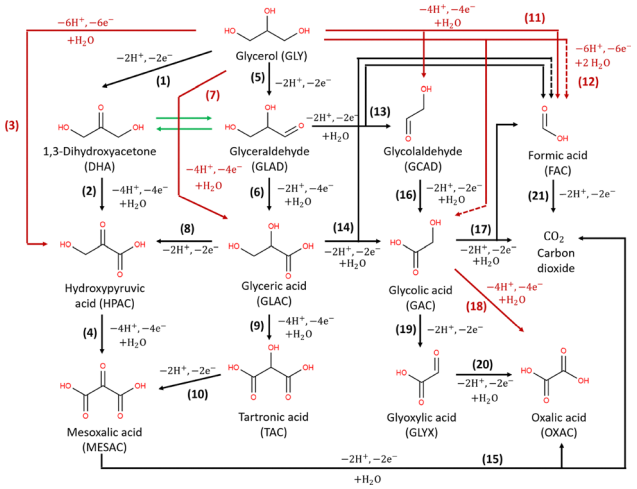

Fig. 1 Glycerol oxidation network adapted from pathways proposed in ref. 15 and 18–20. Black lines represent stepwise oxidation of glycerol and its intermediates; red lines denote direct oxidation routes to final products without intermediate formation; and green arrows indicate the equilibrium isomerization between dihydroxyacetone (DHA) and glyceraldehyde (GLAD).

Table 1 Sections of the GOR network: (i) OER, (ii) C_3–DHA pathway, (iii) C_3–GLAD pathway, (iv) $C_3 \rightarrow C_2 + C_1$, (v) $C_2 \rightarrow C_2$ or C_1, and (vi) $C_1 \rightarrow C_1$

Section	Number	Reaction	Pathway
i	OER	$H_2O \rightleftharpoons 0.5O_2 + 2H^+ + 2e^-$	OER
ii	1	$GLY \rightleftharpoons DHA + 2H^+ + 2e^-$	C_3–DHA
	2	$DHA + H_2O \rightleftharpoons HPAC + 4H^+ + 4e^-$	
	3	$GLY + H_2O \rightleftharpoons HPAC + 6H^+ + 6e^-$	
	4	$HPAC + H_2O \rightleftharpoons MESAC + 4H^+ + 4e^-$	
iii	5	$GLY \rightleftharpoons GLAD + 2H^+ + 2e^-$	C_3–GLAD
	6	$GLAD + H_2O \rightleftharpoons GLAC + 2H^+ + 2e^-$	
	7	$GLY + H_2O \rightleftharpoons GLAC + 4H^+ + 4e^-$	
	8	$GLAC \rightleftharpoons HPAC + 2H^+ + 2e^-$	
	9	$GLAC + H_2O \rightleftharpoons TAC + 4H^+ + 4e^-$	
	10	$TAC \rightleftharpoons MESAC + 2H^+ + 2e^-$	
iv	11	$GLY + H_2O \rightleftharpoons GCAD + FAC + 4H^+ + 4e^-$	$C_3 \rightarrow C_2 + C_1$
	12	$GLY + 2H_2O \rightleftharpoons GAC + FAC + 6H^+ + 6e^-$	
	13	$GLAD + H_2O \rightleftharpoons GCAD + FAC + 2H^+ + 2e^-$	
	14	$GLAC + H_2O \rightleftharpoons GAC + FAC + 2H^+ + 2e^-$	
	15	$MESAC + H_2O \rightleftharpoons OXAC + CO_2 + 2H^+ + 2e^-$	
v	16	$GCAD + H_2O \rightleftharpoons GAC + 2H^+ + 2e^-$	$C_2 \rightarrow C_2$ or
	17	$GAC + H_2O \rightleftharpoons FAC + CO_2 + 2H^+ + 2e^-$	C_1
	18	$GAC + H_2O \rightleftharpoons OXAC + 4H^+ + 4e^-$	
	19	$GAC \rightleftharpoons GLYX + 2H^+ + 2e^-$	
	20	$GLYX + H_2O \rightleftharpoons OXAC + 2H^+ + 2e^-$	
vi	21	$FAC \rightleftharpoons CO_2 + 2H^+ + 2e^-$	$C_1 \rightarrow C_1$

and the electrolyte. The process is thermodynamically driven by the difference between the Fermi level of the electrode (or quasi-Fermi level of holes for photoanodes) and the electrochemical potential of the redox couple. The adsorption configuration of glycerol on the catalyst surface governs the formation of the initial C_3 oxidation products and the subsequent reaction pathway. These primary species can undergo further oxidation *via* (i) desorption, re-adsorption and oxidation, (ii) continuous surface-bound oxidation, or (iii) a combination of both routes (Fig. 1). In the first pathway, hereafter referred as sequential route (black arrows), adsorbed glycerol is initially oxidized to DHA or GLAD, which then desorb from the surface and re-adsorb for further oxidation to other C_3, C_2 and C_1 molecules. In the continuous surface-bound oxidation (red arrows), the intermediate remains anchored to the surface and undergoes successive oxidation steps without desorption, thereby suppressing the release of intermediate molecules. Both mechanisms usually coexist, and their relative importance depends on adsorption strength, applied potential, and temperature—factors that critically influence product selectivity.

Regarding the homogeneous reactions, these usually are undesired side reactions that compete with the heterogeneous processes. Homogeneous reactions occur in the electrolyte and are driven by the difference in chemical potential between reactants and products, typically requiring thermal energy to overcome activation barriers. These include (i) the interconversion between glyceraldehyde (GLAD) and dihydroxyacetone (DHA) (green arrows, Fig. 1a); (ii) further conversion of GLAD or DHA into smaller molecules such as lactic or acetic acid;[15,16] and (iii) decomposition of unstable products, particularly under strongly alkaline or high-temperature conditions.[17] In this work, we focus exclusively on the isomerization of GLAD and DHA, as these are the primary products of interest.

To facilitate data interpretation, the overall reaction network is divided into six sections (Table 1). These include: (i) OER, representing the energetics of water splitting (for comparison); (ii) the C_3–DHA pathway, corresponding to the left column in Fig. 1, where GLY is oxidized to DHA and related C_3 products up to mesoxalic acid (MESAC); (iii) the C_3–GLAD pathway, shown in the second column of Fig. 1, where GLY is oxidized to GLAD and other C_3 products up to tartronic acid (TAC); (iv) the oxidation of C_3 species into C_2 and C_1 products; (v) the C_2 pathway, depicted in the third column of Fig. 1, involving the oxidation of C_2 compounds into other C_2 or smaller C_1 molecules; and (vi) the oxidation of formic acid to CO_2 ($C_1 \rightarrow C_1$ pathway).

The thermodynamic analysis of the GOR network will start with the standard reversible potential $\left(E^{\circ}_{rev}\right)$ displayed in Fig. 2. Derived from the standard Gibbs free energy of reaction $(\Delta_{rxn}G^{\circ})$, E°_{rev} represents the minimum energy input required for the glycerol oxidation reaction to proceed under standard conditions—298.15 K, 1 bar, pH = 0, and unit activity coefficient. It serves as the primary reference for assessing how other variables influence the thermodynamics of the system. This potential is an intrinsic property of the reaction and does not depend on the nature of the catalyst, the dimensions or shape of the reactor, and the operating conditions besides those fixed in the definition of standard state. As GOR generally produce no gaseous products and is therefore largely insensitive to pressure, except for the oxidation of MESAC, GAC, and FAC to CO_2, pressure effects are neglected in this thermodynamic analysis. Compared to the OER, all GOR pathways require markedly lower energy input, with standard potentials $\left(E^{\circ}_{rev} = \Delta_{rxn}G^{\circ}/nF\right)$ indicating 74 to 96% lower energy demand for endergonic (non-spontaneous) steps and even including several exergonic (spontaneous) transformations. Under these standard conditions, the

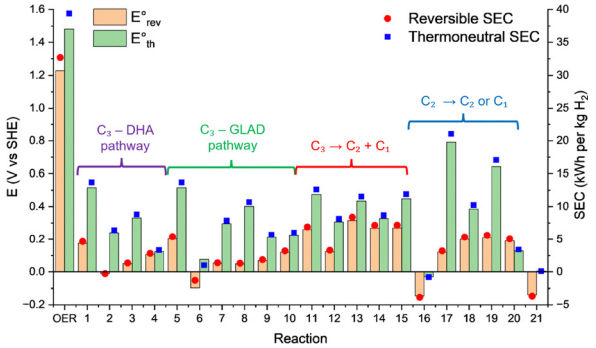

Fig. 2 Reversible (E°_{rev}, orange) and thermoneutral (E°_{th}, green) potentials for the reactions in the GOR network. The secondary *y*-axis shows the specific energy consumption (SEC), calculated from the Gibbs free energy (red squares) and enthalpy (blue squares) of the reactions. To identify the individual reactions within the network, refer to Table 1. By definition of standard conditions, the calculations were performed at room temperature, 25 °C (298 K).

hydrogen evolution reaction (HER) occurs at 0 V *vs.* SHE (referred as V_{SHE} from here onwards), meaning that the overall required potential difference (*i.e.*, voltage) is dictated by the anodic process. Note that under standard conditions, *i.e.*, at pH 0, the SHE and reversible hydrogen electrode (RHE) scales are identical. A positive value indicates that energy must be supplied to the cell for the reaction to proceed, while a negative value indicates that energy is released. Within the C_3 oxidation network, the initial conversion of GLY to DHA or GLAD requires the greatest energy input, with standard potential of 0.18 V_{SHE} and 0.20 V_{SHE}, respectively, while subsequent oxidations of intermediates demand less energy. Interestingly, two direct C_3 oxidation routes, GLY to GLAC (−0.10 V_{SHE}) and GLY to HPAC (−0.01 V_{SHE}), are thermodynamically spontaneous, suggesting potential pathways for efficient hydrogen production without the need of any external energy input. Nonetheless, these reactions have not been studied or harnessed for energy and chemical production, likely due to the need of large overpotentials to overcome kinetic barriers under realistic operating conditions. Compared to the C_3 pathway, oxidative C–C bond cleavage leading to C_2 and C_1 products generally requires a higher energy input, reflecting the additional energetic cost of bond breaking. Notable exceptions are the oxidations of GLY to FAC and GAC, both with standard potentials around 0.12 V_{SHE}—comparable to the initial C_3 oxidation steps. Further oxidation of C_2 intermediates is typically thermodynamically unfavourable, except for the oxidation of GCAD to GAC, which is spontaneous, consistent with aldehyde-to-acid transformations observed in other parts of the network. Similarly, the final oxidation of FAC to CO_2 is strongly exergonic, indicated by its negative reversible potential.

The proximity of the different standard potentials across the reaction network highlights the intrinsic challenge of achieving high product selectivity, as already reported in our previous investigation.[7] For instance, operating near the reversible potential to produce DHA or GLAD can minimize side reactions, mostly from the $C_3 \rightarrow C_2 + C_1$ pathway, but yields unpractical low production rates. Increasing the applied potential enhances reaction rates but simultaneously activates competing pathways. Besides, reactions with lower reversible potentials than DHA or GLAD will experience higher applied overpotentials, increasing their production rate and ultimately compromising selectivity.

To establish a more realistic bound for the applied potential, the thermoneutral voltage ($E^{\circ}_{th} = \Delta_{rxn}H^{\circ}/nF$) was determined. This parameter, derived from the standard reaction enthalpy ($\Delta_{rxn}H^{\circ}$), offers a practical estimate of the minimum voltage to operate the device under isothermal conditions in an adiabatic system, and serves as a lower bound for the total energy demand of the electrolytic cell.[21] For instance, when endothermic reactions occur in a system operating below the corresponding E°_{th}, additional energy must be supplied in the form of heat to keep the working temperature constant, thus increasing the overall energy consumption of the process. Because most glycerol oxidation reactions are endothermic, E°_{th} is higher than the corresponding E°_{rev}, reflecting an increased energetic requirement. For reactions in the C_3 oxidation pathway, this difference is particularly pronounced, with thermoneutral potentials rising by 18–715% relative to their reversible values. For example, the potential difference for GLY ⇌ DHA increases from 0.18 V to 0.51 V (+193%), for GLY ⇌ GLAD from 0.20 V to 0.51 V (+153%), and for GLAC ⇌ HPAC from 0.05 V to 0.40 V (+700%). Reactions involving C–C bond cleavage exhibit more moderate increases (21–146%), while C_2 oxidation steps display broader variability, ranging from 33% to 553%, and reaching the network's maximum potential difference of 0.79 V for GAC ⇌ FAC + CO_2. Although these results reveal greater disparities between reactions when thermoneutral voltages are considered, achieving high selectivity remains challenging. For instance, the direct oxidations of GLY to DHA or GLAD require higher thermoneutral voltages than most competing pathways, restricting selective operation. In contrast, the GLAD ⇌ GLAC and GCAD ⇌ GAC transformations exhibit notably lower thermoneutral voltages, suggesting they could enable more selective (photo)electrochemical oxidation—albeit with limited economic incentive, given the lower market value of their products relative to the reactants.

To highlight the energy efficiency of the GOR in comparison to the OER for hydrogen production, the theoretical specific energy consumption (SEC) was calculated. Eqn (7) quantifies the energy required to generate 1 kg of H_2:

$$\mathrm{SEC} = \frac{\Delta_{rxn}G^{\circ} \text{ or } \Delta_{rxn}H^{\circ}\ (\mathrm{J\ mol^{-1}})}{\text{moles of } H_2 \text{ produced} \cdot H_2 \text{ molar mass } (\mathrm{kg\ mol^{-1}})} \times \frac{1\ \mathrm{kWh}}{3.6 \times 10^{6}\ \mathrm{J}} \quad (7)$$

In water electrolysis, the SEC is 32.7 kWh $(\mathrm{kg\ H_2})^{-1}$ when calculated from the reversible potentials, and 39.4 kWh $(\mathrm{kg\ H_2})^{-1}$ when based on the thermoneutral voltage. In practice, however, commercial electrolysers typically operate at higher values, consuming between 55 and 70 kWh $(\mathrm{kg\ H_2})^{-1}$.[22] In contrast, the calculated SEC for the GOR is significantly lower, ranging

from −3.8 to 8.4 kWh $(kg\ H_2)^{-1}$ calculated with the reversible potentials, and from −0.81 to 21 kWh $(kg\ H_2)^{-1}$ when using the thermoneutral voltage. These results illustrate the energetic advantage of substituting the oxygen evolution reaction with glycerol oxidation, offering a substantial reduction in hydrogen production costs—or, more broadly, in the energy demand of any cathodic process coupled to GOR. Consequently, the GOR emerges as a highly promising route for improving the overall energy efficiency of (photo)electrolytic processes.

Now that the energetic requirements at room temperature have been assessed, we turn to the effect of temperature. Its influence on GOR appears mainly as a gradual decrease in the required voltage with rising temperature, reflecting the generally endothermic character of the reactions. As illustrated in Fig. 3, the extent of this temperature dependence varies considerably across the reaction network. Within the C_3 pathway, the direct oxidations of GLY to DHA and GLAD display a pronounced temperature sensitivity: the reversible potential decreases from 0.18 V_{SHE} at 25 °C to 0.10 V_{SHE} at 80 °C for DHA, and from 0.20 V_{SHE} to 0.07 V_{SHE} for GLAD. Most of the reactions in this pathway preserve their spontaneity or non-spontaneity character throughout the studied temperature range, except for the GLAC ⇌ HPAC reaction, which becomes spontaneous at elevated temperatures. For C–C bond cleavage, all processes remain endergonic but exhibit moderate decreases in their half-reaction potential, typically around 9%. Similarly, C_2 oxidation reactions that are non-spontaneous at ambient temperature remain thermodynamically unfavourable but require less energy input as temperature rises. Conversely, spontaneous steps become increasingly exergonic, strengthening the thermodynamic drive toward product formation. Among these, the oxidation of formic acid (FAC) to CO_2 becomes the most exergonic process in the network at higher temperatures.

Despite these thermal effects, the reversible potentials associated with the formation of desired products remain higher than those of competing side reactions, indicating that temperature alone cannot effectively tune selectivity. Furthermore, interfacial phenomena—such as adsorption–desorption equilibria and other kinetic effects not captured in this thermodynamic framework—may further influence the real temperature response. Regarding the effect of pH, its influence on the GOR arises from the acid–base properties of the intermediates and the number of hydronium ions generated or consumed during the reaction. Fig. 4 and 5 illustrate how variations in pH affect the reversible half-reaction potentials of the GOR network. Over the entire pH range, all glycerol oxidation pathways show markedly less positive potentials than the OER. For the OER reaction, the potential decreases from 1.229 V_{SHE} at pH 0 to 0.401 V_{SHE} at pH 14, following a slope of −59 mV per pH unit. These values are substantially more positive than the GOR potentials (and not plotted in Fig. 4 and 5 because they are off-scale). For the GOR pathways, the pH dependence of the reversible potential is primarily governed by the third term of eqn (S6), with a slope of $-59 \cdot h \cdot n_e^{-1}$ mV per pH unit, where h represents the stoichiometric coefficient of H^+ and n_e the number of electrons transferred per oxidized molecule. In the case of the hydrogen evolution reaction (HER) and for reactions involving species with high pK_a values, the potential–pH slope remains nearly constant across the entire range until deprotonation becomes significant. This behaviour is observed, for instance, in the oxidation of glycerol (pK_a ≈ 14.15[23]) to glyceraldehyde (pK_a ≈ 12.84[24]) or dihydroxyacetone (pK_a ≈ 13.5[25]) which displays a change in slope only under strongly

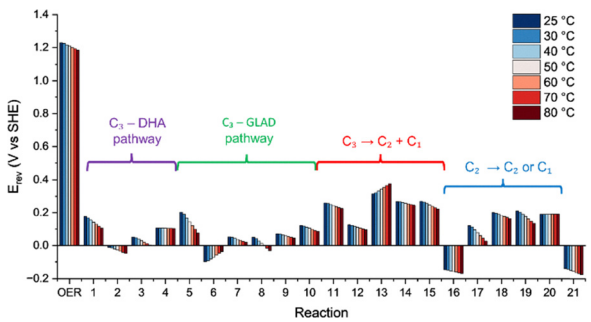

Fig. 3 Effect of temperature (25–80 °C) on the reversible potentials of the reactions in the GOR network. Colours indicate temperature, ranging from blue (25 °C) to red (80 °C). To identify the individual reactions within the network, refer to Table 1. Note that $E_{rev} = E^{\circ}_{rev}$ only for T = 25 °C (298 K), as by definition of standard conditions.

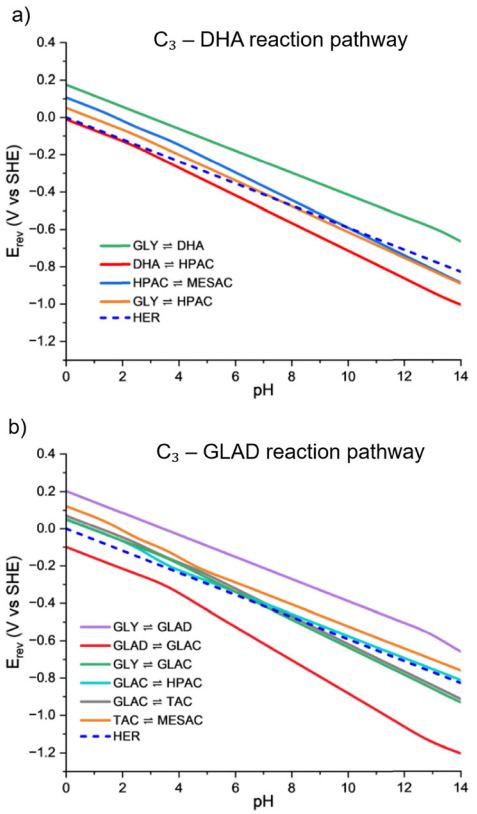

Fig. 4 Potential-pH relationships at 25 °C (298 K) for the different reactions of the GOR network for the C_3 reaction pathway: (a) DHA pathway, (b) GLAD pathway. Solid lines correspond to the oxidation reactions. The blue dashed line corresponds to the coupled cathodic reaction, in this case HER. Enlarged version of this plot can be found in the SI, Fig. S14 and S15.

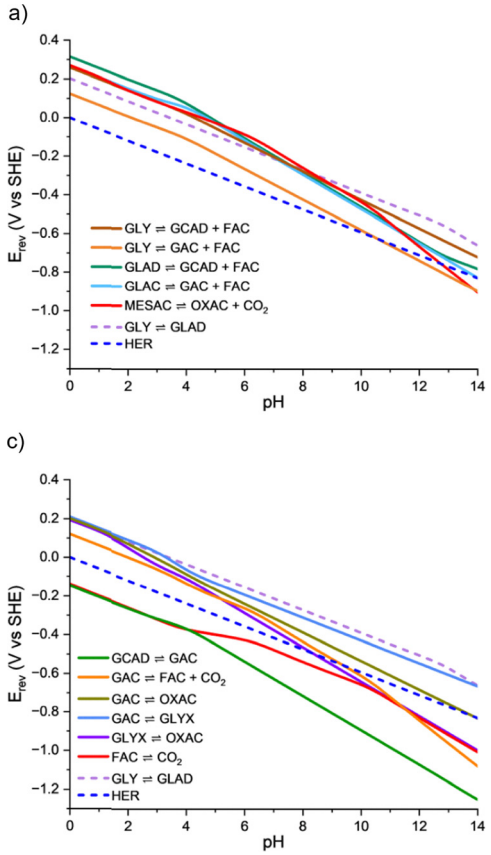

Fig. 5 Potential-pH relationships at 25 °C (298 K) for the different reactions of the GOR network for the formation of C_2 and C_1 molecules: (a) oxidation of C_3 to C_2 and C_1 pathway, (b) oxidation of C_2 to C_2 and C_1 pathway. Solid lines correspond to the oxidation reactions. The blue dashed line corresponds to the coupled cathodic reaction, in this case HER. The light purple dashed line corresponds to the oxidation of GLY to GLAD, a reference point for comparison with the C_3 to C_3 transformations. Enlarged version of this plot can be found in the SI, Fig. S16 and S17.

alkaline conditions (pH > 12). In contrast, reactions in which either the reactants or products are acids exhibit a much stronger pH dependence. In these cases, distinct slope changes appear near the pK_a values of the involved species, reflecting the transition between the protonated and deprotonated forms that alters the energetics of the reaction.

For (photo)electrolytic devices, the cell voltage (E_{cell}, eqn (8)) is given by the sum of the thermoneutral potential E°_{th} of the k-th reaction, the corresponding kinetic overpotential ($\eta_{ox,k}$), and the unavoidable ohmic losses in the system (ΔE_{loss}). The latter must be quantified case-by-case, as it strongly depends on the concentration and type of the supporting electrolyte used, the geometry of the device, the presence of a compartment separator, and eventual accumulation of H_2 bubbles at the cathode.

$$E_{cell} = \left[E^{\circ}_{th,k} + \eta_{ox,k}\right] + \eta_{HER} + \Delta E_{loss} \quad (8)$$

Note that, assuming proton transport through the device from anode to cathode is sufficiently fast to close the circuit (*i.e.* protons are the current-carrying ions), the cathodic process for any of the GORs is proton reduction (HER). Hence, $\eta_{red,k} = \eta_{HER}\ \forall\ k$.

Since this work focuses only on thermodynamics, it is not possible to quantify the needed overpotential and other ohmic losses. However, the thermodynamic contribution to the cell voltage can be assessed, as it is given by the difference between the lines representing the GOR and the HER. As before, a positive value indicates that energy must be supplied to the system, whereas a negative value indicates that the reaction is exergonic and releases energy. Starting with the C_3 pathway, most reactions are thermodynamically unfavourable at pH 0, as observed in Fig. 4. The oxidation of GLY to DHA or GLAD requires higher voltages than other C_3 oxidation routes; thus, any voltage sufficient to drive these target reactions will also activate lower-potential competing pathways. As a result, side reactions proceed simultaneously—often under excess applied overpotential—hindering selectivity toward DHA and GLAD. With increasing pH, the oxidation potentials of most reactions within the C_3 network decrease with a steeper slope than the GLY ⇌ DHA, GLY ⇌ GLAD and HER lines, indicating a stronger effect of pH. Around neutral conditions (pH = 7), many oxidation potentials approach the HER line, and at highly alkaline pH, they even fall below it. Therefore, as pH rises, the oxidation of GLY and the re-oxidation of its products become less energetically demanding, and in some cases even spontaneous (when falling below the HER line). For the C_3 pathway, this transition from non-spontaneous to spontaneous behaviour occurs for the transformations GLY ⇌ HPAC, GLY ⇌ GLAC, DHA ⇌ HPAC, GLAD ⇌ GLAC, HPAC ⇌ MESAC, and GLAC ⇌ TAC. However, the cell potential for the formation DHA/GLAD remains nearly unchanged throughout the pH range. Consequently, if the aim is to produce these molecules, competing pathways will become more thermodynamically and kinetically favoured in alkaline environments. The widening gap between the DHA or GLAD lines and those of the competing reactions with increasing pH reflects the growing overpotential available to drive these side oxidations. For instance, at pH 0, applying a cell voltage of ~0.20 V to oxidize GLY to GLAD provides an overpotential of roughly 0.30 V for the further oxidation of GLAD to GLAC (Fig. 4b). Likewise, oxidizing GLY to DHA at its standard potential difference (~0.18 V) gives an overpotential of 0.19 V for the subsequent oxidation of DHA to HPAC (Fig. 4a). At strongly alkaline conditions (pH = 14), maintaining the same applied potentials results in nearly doubled overpotentials—0.66 V and 0.34 V, respectively—significantly increasing the propensity for intermediate over-oxidation. Therefore, higher pH values increase the competition between different reaction pathways and significantly reduce the selectivity toward DHA and GLAD.

For the $C_3 \rightarrow C_2 + C_1$ reaction pathway (Fig. 5a), at acidic pH nearly all reactions—except for the GLY ⇌ GAC + FAC step—require higher potentials than the $C_3 \rightarrow C_3$ oxidations. Their potentials also decrease more steeply with increasing pH due to the formation and subsequent deprotonation of organic acids. However, this pH-driven decrease is generally insufficient

to render the reactions exergonic under highly alkaline conditions, with the exceptions of GLY ⇌ GAC + FAC and MESAC ⇌ OXAC + CO_2. For the $C_2 \rightarrow C_2$ oxidations (Fig. 5b), excluding the GCAD ⇌ GAC reaction, the potentials at acidic pH are comparable to that of GLY ⇌ GLAD and exhibit a similar pH-dependent slope. Above pH 2, however, reactions involving OXAC show a sharp decline in potential owing to the molecule's strong acidity, which enhances proton release, making it more susceptible to changes on pH. The conversion of C_2 or C_1 intermediates to C_1 products is also strongly pH-sensitive: $C_2 \rightarrow C_1$ (GAC ⇌ FAC + CO_2) reactions are endergonic in acidic media but become exergonic under alkaline conditions, while $C_1 \rightarrow C_1$ oxidations (FAC ⇌ CO_2) remain exergonic across the entire pH range, albeit slightly less favourable at pH values above 6 due to the formation of carbonates.

Overall, pathways involving C–C bond cleavage—such as $C_3 \rightarrow C_2 + C_1$ or $C_2 \rightarrow C_1$ transitions—show a much stronger pH dependence than reactions preserving the carbon count. This trend arises from the formation of highly acidic intermediates, notably FAC ($pK_a \approx 3.75$[23]) and GAC ($pK_a \approx 3.83$[23]) as a consequence of bond scission, whose deprotonation increases proton release and thereby increases the influence of the pH on the reaction selectivity.

From a selectivity standpoint, because $C_3 \rightarrow C_2 + C_1$ oxidations demand higher energy input than $C_3 \rightarrow C_3$ conversions under acidic conditions, these undesired pathways can be effectively suppressed by selecting suitable cell voltages and pH values. However, as pH increases, such competing routes become thermodynamically accessible at the potentials required for producing GLAD or DHA. Similarly, the $C_2 \rightarrow C_2$, $C_2 \rightarrow C_1$, and $C_1 \rightarrow C_1$ oxidation reactions remain active under conditions relevant for target product formation, with the available overpotential for these side processes increasing progressively with pH.

An important aspect to highlight is that the effect of pH on the product distribution is inherently dynamic. During GOR at the anode, a pH gradient develops at the electrode surface because of ongoing proton generation. As a result, the reaction environment at the solid/liquid interface becomes more acidic than the bulk solution, despite the diffusion coefficient of protons being larger than the ones of the GOR products. It is therefore worth emphasizing that, although we observe more pronounced shifts in alkaline conditions for $C_2 + C_1$ products, this behaviour will change until a steady state is reached (an equilibrium condition between the proton formation rate at the electrode surface and proton diffusion to the bulk electrolyte). This effect is even more significant in non-buffered systems, where the solution cannot effectively counteract these pH variations. Experimentally, the influence of interfacial pH gradients on product selectivity can be minimized by implementing approaches such as the use of highly concentrated buffered electrolytes (*e.g.*, ≥0.1 M phosphate buffers) and enhancing mass transport through controlled hydrodynamic conditions (*e.g.*, stirring).

To further elucidate the influence of pH and potential, Fig. 6 illustrates how the combination of these parameters affects

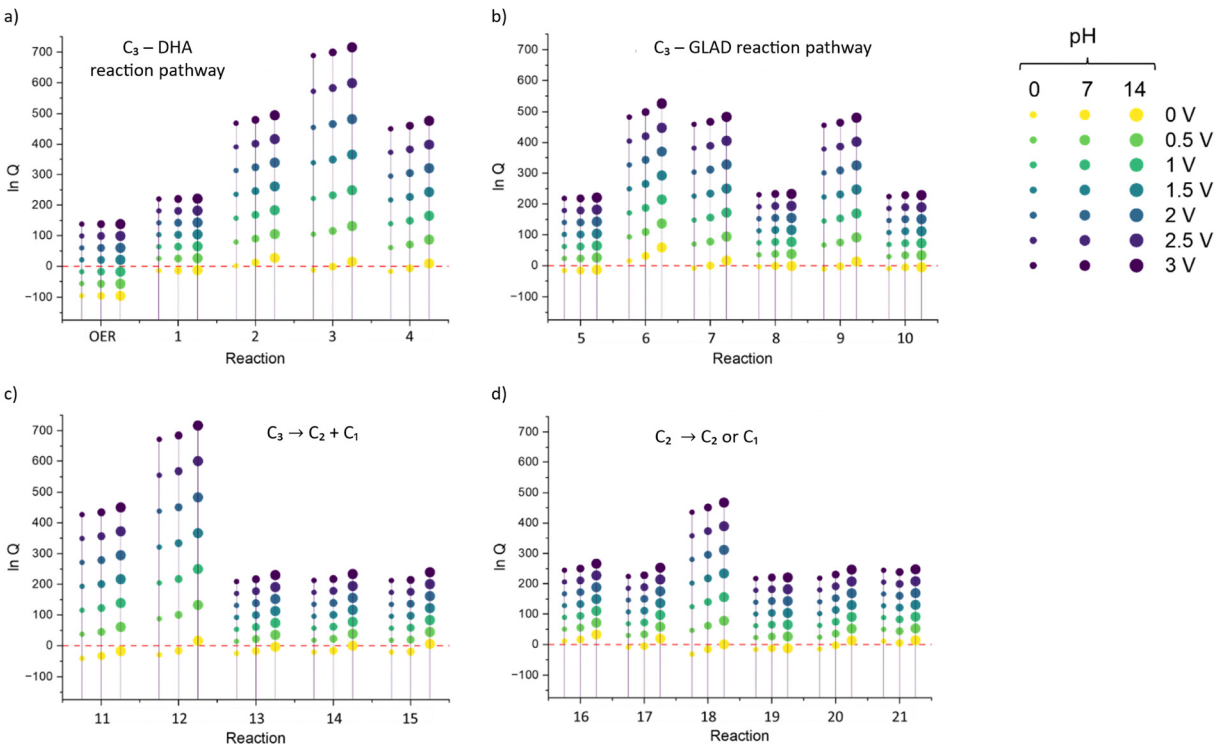

Fig. 6 Effect of applied cell voltage (0–3 V) at 25 °C (298 K) on the natural logarithm of the reaction quotient (ln *Q*) at pH 0, 7, and 14. Each reaction appears as a group of three vertically aligned dot columns, where dot size denotes pH and colour indicates applied potential. pH increases from left to right, and potential from bottom to top. The red dashed line marks ln *Q* = 0. (a) C_3–DHA pathway, (b) C_3–GLAD pathway, (c) oxidation of C_3 to C_2 and C_1 pathway, (d) oxidation of C_2 to C_2 and C_1 pathway. To identify the individual reactions within the network, refer to Table 1.

product selectivity. The plots depict the natural logarithm of the reaction quotient ($\ln Q$) as a function of applied potential (0–3 V) and pH (0, 7, 14), assuming equilibrium conditions governed by the Nernst equation, with HER occurring at the (photo)cathode and either GOR or OER at the (photo)anode. The red dotted line corresponds to $\ln Q = 0$, meaning equal concentration of reactants and products; values above zero reflect increasing product formation while values below zero indicate shift of the reaction towards reactants. For the whole reaction network, two-electron processes—such as water splitting, GLY ⇌ DHA, GLY ⇌ GLAD, GLAC ⇌ HPAC, TAC ⇌ MESAC and most of the C_2 oxidation pathway—show minimal sensitivity to pH and only moderate dependence on applied potential, regardless of pK_a values. In contrast, reactions involving four or more electrons exhibit a pronounced potential dependence that scales with the number of exchanged electrons. For this case, the influence of pH follows the same trends observed in Fig. 5 but is amplified when higher cell voltages are applied. For instance, the six-electron oxidation GLY ⇌ HPAC (reaction #3) shows the most pronounced increase in $\ln Q$ with applied potential. Overall, the pH causes only modest upward shifts in $\ln Q$, and these shifts become meaningful only when reactions involve more than two electrons. The applied potential, however, has a much stronger impact: two-electron steps remain largely unaffected, whereas four- to six-electron reactions respond sharply due to the nF/RT term in eqn (S7), which amplifies the effect of the applied potential.

At higher potentials and more alkaline conditions, multiple competing reactions—especially those involving multi-electron transfers—shift more strongly toward product formation than the desired reactions, resulting in a broader product distribution. For instance, with an applied cell voltage of 0.5 V and assuming the system reaches chemical equilibrium, the reaction shifts toward a diverse set of products (excluding O_2), dominated by HPAC, MESAC, GLAC, TAC, GAC, and FAC. This distribution becomes even more pronounced under alkaline conditions, favouring the formation of many more products. This highlights a central trade-off: while increasing potential and pH improves conversion, it inevitably compromises selectivity by activating parallel reaction routes.

The final parameter influencing the required applied potential—and thus reaction selectivity—is the reactant concentration. This effect is independent of pH and increases or diminishes the applied potential magnitude depending on the degree of conversion (eqn (S6)). Assuming that 0.5 M of reactant is fully converted to product, the oxidation potential of each reaction shifts accordingly (Fig. 7). At the start of the reaction, when no products are present, the potential drops sharply, generating a strong thermodynamic driving force for product formation. Once the first molecules of product appear, the potential rises abruptly and then increases more gradually, with the slope determined by the number of electrons transferred and the reaction stoichiometry. Reactions that form two products while transferring only two electrons exhibit the strongest concentration dependence after and before the initial and final steep changes near 0% and 100% conversion, respectively.

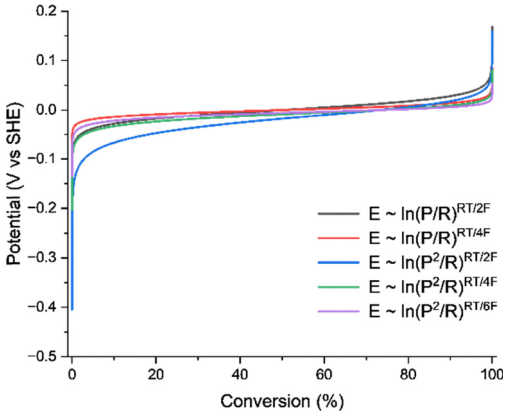

Fig. 7 Effect of reaction conversion on the oxidation potential, which scales with $RT \cdot \ln\left(\frac{\text{Products}}{\text{Reactants}}\right)$ and is normalized by the number of electrons transferred (n) and Faraday's constant (F). The calculations were performed at room temperature, 25 °C (298 K).

In contrast, most other reactions show only moderate shifts of roughly 20–50 mV across a broad concentration range, indicating a relatively weak sensitivity to product accumulation. At higher product concentrations, the potential increases more noticeably, making further oxidation more demanding and preventing complete conversion. A more concrete example of this trend is displayed in Fig. S18 with the effect of concentration on the oxidation of GLY ⇌ DHA, GLY ⇌ GLAC, GLAC ⇌ FAC + GAC, GLY ⇌ GCAD + FAC and GLY ⇌ GAC + FAC, illustrating all the cases displayed in Fig. 7. The steep potential changes at very low or very high conversions arise from entropic effects: systems composed almost entirely of reactants or products have lower entropy than mixtures, producing larger variations in Gibbs free energy and, consequently, in the electrochemical potential.

Because DHA and GLAD are among the most commonly targeted GOR products, it is important to note that they can undergo acid- or base-catalysed isomerization reactions[26] (green arrows in Fig. 1). This means that, beyond the competing electrochemical pathways converting GLAD or DHA, a homogeneous reaction in solution also affects their concentrations. As shown in Fig. 8, DHA is the predominant isomer across the entire pH range up to 12, appearing at levels 8.5–10 times higher than GLAD. In strongly alkaline conditions (pH > 12), however, this ratio drops sharply to about 1.6–2.0. This behaviour arises from the energy differences between the protonated and deprotonated species involved. Below pH 10, only the protonated forms participate, and the energy gap between GLAD and DHA remains constant, yielding a flat trend. Around pH 10, GLAD begins to deprotonate ($pK_a \approx 12.84$,[24] Fig. S6), forming an anion that is thermodynamically less favourable than DHA, thereby shifting the equilibrium further toward DHA. At higher pH, DHA also starts to deprotonate ($pK_a \approx 13.5$,[25] Fig. S1). Because the energy difference between the anionic forms is smaller than that between their protonated counterparts, the equilibrium constant responds accordingly and decreases sharply. Thus, depending on the target product,

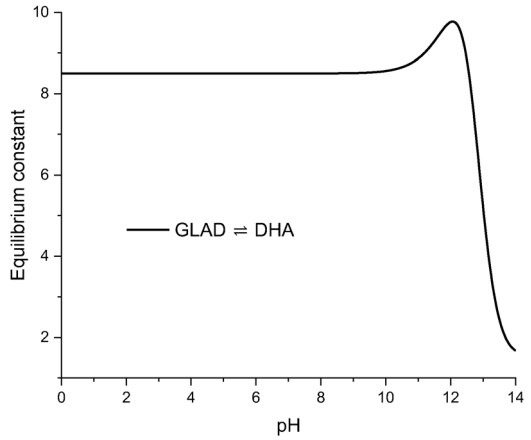

Fig. 8 Equilibrium constant for the GLAD-to-DHA isomerization reaction as a function of pH at 25 °C (298 K).

selecting an appropriate pH is essential for steering the isomerization equilibrium in solution.

It is important to note that the results presented here are purely thermodynamic, based on chemical equilibrium calculations, and do not incorporate any electrokinetic aspects of the reactions. In practice, the balance between thermodynamic and kinetic control likely plays a central role in determining selectivity. Other relevant factors are also not included, such as electrolyte–solute interactions (known to influence activity and selectivity[27,28]), double-layer effects on electrocatalytic behavior,[29] mass transport and hydrodynamics near the working electrode (which can modify selectivity[30]), and adsorption or interaction modes (which likewise affect product distribution[20]). Despite these limitations, the thermodynamic trends reported here align with experimental observations and provide a useful framework for assessing how reaction conditions shape selectivity.

Conclusions

This study provides a full thermodynamic evaluation of the GOR and its associated reaction network. Although most pathways are endergonic, all require far less energy than the OER, with reversible and thermoneutral cell voltages reduced by 74–96% and 46–94%, respectively (assuming the GOR is combined with the HER at the cathode). Consequently, replacing OER with GOR lowers the theoretical SEC for H_2 production to −0.81–21 kWh (kg H_2)$^{-1}$ under thermoneutral conditions. However, the reversible potentials of most individual pathways cluster closely together across the temperature range, and the desired products (DHA and GLAD) consistently require higher driving forces than many competing reactions. Thus, temperature alone does not offer meaningful thermodynamic leverage for selectivity. pH effects are more pronounced—favouring product formation in alkaline conditions, especially for reactions involving proton release—but these conditions primarily promote side reactions. A more positive applied potential strongly influences the equilibrium of any multi-electron pathway but also benefits competing transformations. Concentration effects, dominated by entropy, favour product formation only at very low conversions and impede full conversion at high product buildup, with intermediate regions showing modest shifts of 20–50 mV. Overall, while GOR provides clear energetic advantages over OER, our thermodynamic analysis reveals that selectivity cannot be controlled through temperature, pH, potential, or concentration, under equilibrium conditions. Alkaline environments and high potentials lead to side-reaction pathways, making them unfavourable operating conditions for selective oxidation to C_3 products (*i.e.* DHA, GLAD, and GLAC). To limit the activation of side reactions it is therefore recommended to operate in acidic media, at mild potentials (below +1.23 V *vs.* RHE), and preferentially at room temperature. These findings highlight the need to integrate kinetic, catalytic, and interfacial considerations alongside thermodynamics to effectively steer selectivity in GOR.

Author contributions

A. F. P.-T.: conceptualization, data curation, formal analysis, methodology, visualization, writing – original draft, writing – review & editing; R. v. d. K.: resources, supervision, validation, writing – review & editing; M. F.: funding acquisition, investigation, project administration, resources, supervision, validation, writing – review & editing.

Conflicts of interest

There are no conflicts to declare.

Acronyms

PEC	Photoelectrochemistry
OER	Oxygen evolution reaction
HER	Hydrogen evolution reaction
GOR	Glycerol oxidation reaction
SEC	Specific energy consumption
GLY	Glycerol (C_3)
DHA	1,3-Dihydroxyacetone (C_3)
GLAD	Glyceraldehyde (C_3)
HPAC	Hydroxypyruvic acid (C_3)
GLAC	Glyceric acid (C_3)
MESAC	Mesoxalic acid (C_3)
TAC	Tartronic acid (C_3)
GCAD	Glycolaldehyde (C_2)
GAC	Glycolic acid (C_2)
GLYX	Glyoxylic acid (C_2)
OXAC	Oxalic acid (C_2)
FAC	Formic acid (C_1)
CO_2	Carbon dioxide (C_1)

Data availability

The data reported in this manuscript and in the supplementary information (SI) can be obtained from the corresponding authors upon reasonable request. Supplementary information including details about the derivation of the thermodynamic model and speciation plots for the glycerol oxidation reaction pathways discussed in this work is available. See DOI: https://doi.org/10.1039/d5cp05002b.

Acknowledgements

This work was supported by the European Innovation Council (EIC) *via* OHPERA (grant agreement 101071010) and co-funded by the European Union under grant agreement 101137889 (PH2OTOGEN). Views and opinions expressed are however those of the authors only and do not necessarily reflect those of the European Union or Clean Hydrogen JU. Neither the European Union nor the granting authority can be held responsible for them. The project is supported by the Clean Hydrogen Partnership and its members.

Notes and references

1 Z. Fan, W. Zhang, L. Li, Y. Wang, Y. Zou, S. Wang and Z. Chen, *Green Chem.*, 2022, **24**, 7818–7868.
2 C. M. Pichler, *ChemCatChem*, 2023, **15**, e202300648.
3 H. Luo, J. Barrio, N. Sunny, A. Li, L. Steier, N. Shah, I. E. Stephens and M.-M. Titirici, *Adv. Energy Mater.*, 2021, **11**, 2101180.
4 T. Kahlstorf, J. N. Hausmann, T. Sontheimer and P. W. Menezes, *Global Challenges*, 2023, **7**, 2200242.
5 M. S. E. Houache, K. Hughes and E. A. Baranova, *Sustainable Energy Fuels*, 2019, **3**, 1892–1915.
6 M. Yoo, D. Choi, M. Shin, S. Jung, J. Lee and H. J. Kim, *Chem. Eng. J.*, 2025, **518**, 164743.
7 A. F. Pérez-Torres, H. Kong, F. F. Abdi, R. van de Krol and M. Favaro, *Chem. Commun.*, 2025, **61**, 2083–2086.
8 K. Zhu, X. Zhang, L. Wen, S. Zhou, D. S. Achilleos, R. Amal, Y. H. Ng and F. F. Abdi, *Nat. Rev. Clean Technol.*, 2025, 1–17.
9 Mike, Glycerol price index, https://businessanalytiq.com/procurementanalytics/index/glycerol-price-index/, (accessed December 18, 2025).
10 News Release, https://globenewswire.online/news-release-global-dihydroxyacetone-production-analysis-import-export-price-update-2025/, (accessed December 18, 2025).
11 W. Zhang, B. Hao, Q. Gao, Y. Wang, X. Bian, H. Gong, R. Tian, A. Wei, J. Wang and Y. Liu, *Appl. Catal., A*, 2025, **697**, 120205.
12 L. Wen, X. Zhang and F. F. Abdi, *Mater. Today Energy*, 2024, **44**, 101648.
13 E. C. Carlson, *Chem. Eng. Prog.*, 1996, **92**, 35–46.
14 Inc. Aspen Technology, *Aspen Plus extregistered Physical Property Methods and Models (Version 11.1)*, Aspen Technology, Inc., Bedford, MA, 2021.
15 X. Hu, J. Lu, Y. Liu, L. Chen, X. Zhang and H. Wang, *Environ. Chem. Lett.*, 2023, **21**, 2825–2861.
16 E. Jolimaitre, D. Delcroix, N. Essayem, C. Pinel and M. Besson, *Catal. Sci. Technol.*, 2018, **8**, 1349–1356.
17 M. K. Goetz, M. T. Bender and K.-S. Choi, *Nat. Commun.*, 2022, **13**, 5848.
18 T. Hamada, A. R. Circelli, H. Inoue, C. A. Randall and E. L. Clark, *J. Phys. Chem. C*, 2024, **128**, 10790–10801.
19 H. Sheng, A. N. Janes, R. D. Ross, H. Hofstetter, K. Lee, J. R. Schmidt and S. Jin, *Nat. Catal.*, 2022, **5**, 716–725.
20 T. Li and D. A. Harrington, *ChemSusChem*, 2021, **14**, 1472–1495.
21 K. M. Ebeling, D. Bongartz, S. Mürtz, R. Palkovits and A. Mitsos, *Ind. Eng. Chem. Res.*, 2024, **63**, 8250–8260.
22 M. Chatenet, B. G. Pollet, D. R. Dekel, F. Dionigi, J. Deseure, P. Millet, R. D. Braatz, M. Z. Bazant, M. Eikerling, I. Staffell, P. Balcombe, Y. Shao-Horn and H. Schäfer, *Chem. Soc. Rev.*, 2022, **51**, 4583–4762.
23 *CRC Handbook of Chemistry and Physics*, ed. W. M. Haynes, CRC Press, 95th edn, 2014.
24 D-glyceraldehyde (YMDB00575) – Yeast Metabolome Database, https://www.ymdb.ca/compounds/YMDB00575, (accessed June 24, 2025).
25 Dihydroxyacetone, https://go.drugbank.com/drugs/DB01775, (accessed June 24, 2025).
26 L. Bricotte, K. Chougrani, V. Alard, V. Ladmiral and S. Caillol, *Molecules*, 2023, **28**, 2724.
27 X. Huang, Y. Zou and J. Jiang, *ACS Sustainable Chem. Eng.*, 2021, **9**, 14470–14479.
28 H. Kong, S. Gupta, A. F. Pérez-Torres, C. Höhn, P. Bogdanoff, M. T. Mayer, R. van de Krol, M. Favaro and F. F. Abdi, *Chem. Sci.*, 2024, **15**, 10425–10435.
29 P. Li, Y. Jiao, J. Huang and S. Chen, *JACS Au*, 2023, **3**, 2640–2659.
30 N. B. Watkins, Z. J. Schiffer, Y. Lai, C. B. I. Musgrave, H. A. Atwater, W. A. I. Goddard, T. Agapie, J. C. Peters and J. M. Gregoire, *ACS Energy Lett.*, 2023, **8**, 2185–2192.

